Journal of Colloid and Interface Science 529 (2018) 234–242

Contents lists available at ScienceDirect

Journal of Colloid and Interface Science

journal homepage: www.elsevier.com/locate/jcis

Regular Article

pH-modulated self-assembly of colloidal nanoparticles in a dual-droplet inkjet printing process

Karam Nashwan Al-Milaji [a], Vinod Radhakrishnan [b], Prajakta Kamerkar [b], Hong Zhao [a,*]

[a] Virginia Commonwealth University, Department of Mechanical and Nuclear Engineering, BioTech One, 800 East Leigh Street, Richmond, VA 23219, USA
[b] Anton Paar USA, Inc., 10215 Timber Ridge Dr., Ashland, VA 23005, USA

GRAPHICAL ABSTRACT

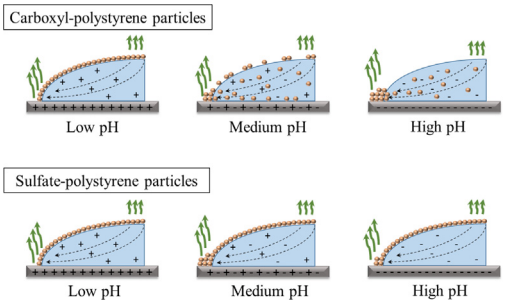

ARTICLE INFO

Article history:
Received 8 April 2018
Revised 3 June 2018
Accepted 4 June 2018
Available online 5 June 2018

Keywords:
Dual-droplet inkjet printing
pH-modulation
Interfacial self-assembly
Deposition of colloidal nanoparticles

ABSTRACT

Hypothesis: Interfacial self-assembly has been demonstrated as a powerful driving mechanism for creating various nanostructured assemblies. In this work, we employed a dual-droplet printing process and interfacial self-assembly mechanism to produce deposits with controlled assembly structures of colloidal nanoparticles. We hypothesize that pH modulation of the droplet will influence the interfacial self-assembly through the multibody interactions, e.g. particle-particle, particle-interface, and particle-substrate interactions, correspondingly affecting the deposition morphology of the colloidal nanoparticles.
Experiments: During the dual-droplet printing, a wetting droplet, containing colloidal nanoparticles, was jetted over a supporting droplet that contains water only. pH modulation was carried out to the supporting droplet. The self-assembly of two kinds of functionalized polystyrene (PS) nanoparticles (carboxyl-PS and sulfate-PS) was systematically investigated under various pH conditions.
Findings: Depending on the pH level of the supporting droplet, deposits of carboxyl-PS particles ranging from clear ring-like patterns to nearly uniform monolayer depositions have been obtained. On the other hand, the sulfate-PS particles, even at extreme basic and acidic environments, successfully assemble into nearly monolayer depositions. The multibody interactions are discussed. Such findings can be harnessed in manufacturing high-performance optical and electronic devices.

1. Introduction

Deposits acquired by evaporation of particle-laden droplets and films with controlled assembly are of considerable importance in fundamental science and engineering that influence a variety of technologies ranging from thin film coatings to printing functional devices [1–3]. Recently, the evaporation-induced self-assembly process has received much attention as a technique that enables control over deposits to produce high-quality planar colloidal crystal films [4,5]. However, the formation of ring-shaped deposits during evaporation process, especially when the three-phase contact

* Corresponding author.
E-mail address: hzhao2@vcu.edu (H. Zhao).

https://doi.org/10.1016/j.jcis.2018.06.008
0021-9797/

lines of the particle-laden sessile droplets are pinned, makes this phenomenon rather complicated [6]. The evaporation of sessile droplets is a non-equilibrium process. The complex fluid dynamics of a droplet stems from the non-uniform evaporation flux of the solvent over its liquid-vapor interface [7,8]. As a result, the suspended particles are driven to the droplet edge by the action of evaporation-induced flow forming this ubiquitous ring-like pattern, known as the coffee-ring effect [9,10]. Significant research efforts have been devoted to mitigate or suppress the coffee-ring formation by means of, controlling the drying conditions of solvents (e.g., substrate temperature [11], relative humidity [12], and volatile solvents [13]), modifying particle shapes [14,15], adjusting substrate wettability [16,17], and intentionally inducing Marangoni flow due to surface tension gradient that is generated by temperature difference across the interface, surfactant, or cosolvent [18–22], etc. It is worth noting that the coffee-ring effect is considered as a detrimental defect in printing and coating technologies; nonetheless, this stain phenomenon has been harnessed in a number of technological applications [23–25].

Among the research endeavors in tuning deposits of colloidal sessile droplets, Bharadwaj et al. [26] experimentally investigated the role of Derjanguin-Landau-Verwey-Overbeek (DLVO) interactions on deposits left by evaporating sessile droplets containing titania nanoparticles on a glass substrate. As the pH of the solution changes, the morphology of nanoparticle deposits varies accordingly from rings to uniform disks. Devineau et al. [27] analyzed the deposit morphology of drying droplets containing protein-functionalized polystyrene (PS) particles with different surface properties. Protein adsorption on the surface of the suspended particles alters the surface charge of the PS particles. The authors assert that the coffee-ring effect can be suppressed when the particles are neutralized by the protein adsorption.

Even though an immense experimental and theoretical work have been diligently undertaken to improve the understanding of drying mechanism and pattern formation upon evaporation of particle-laden sessile droplets [28], not much attention has been given to creating uniform depositions with nearly a monolayer of self-assembled colloidal particles. Very recently, we have demonstrated the ability to produce a well-ordered assembly of a nearly monolayer of PS nanoparticles by employing a dual-droplet inkjet printing process [29]. By tuning the surface tension, droplet size, and droplet speed, a wetting droplet that contains PS nanoparticles successfully spreads on the surface of a supporting droplet. In this study, we investigate the effect of pH modulation of the supporting droplet on the nanoparticle depositions as a result of particle-particle interactions, particle-interface interactions, and particle-substrate interactions. Negatively charged PS particles with different surface functionalization groups were utilized and the electrostatic interactions were tuned via the pH value of the supporting droplet. This study uncovers a facile technique to control the colloidal assembly upon solvent evaporation in enormous industrial and research applications, especially for inkjet printing, coating processes, and fabricating functional devices involving liquid processing of colloidal inks.

2. Materials and methods

2.1. Materials

Microscope glass slides (25 mm × 75 mm), sodium hydroxide solution (10.0 N), and KOPTEC ethanol (99.5% purity) were obtained from VWR. Sulfate latex beads (8% w/v, 0.1 μm) and carboxyl latex beads (4% w/v, 0.1 μm) were purchased from Thermo Fisher Scientific. Tris(hydroxymethyl)aminomethane (Tris) 99.8% purity, 2-(3,4-Dihydroxyphenyl)ethylamine hydrochloride (dopamine), and hydrochloric acid (37% purity) were acquired from Sigma-Aldrich. Deionized (DI) water with a resistivity of 18.2 MΩ × cm was produced by Direct-Q water purification system (Millipore Sigma). All chemicals were used as received without further purification.

2.2. Substrate treatment

All glass substrates were first cleaned with solvents following the order of hot soapy water, acetone, and Isopropanol, then rinsed with DI water and dried by clean compressed air. The cleaned substrates were further treated with plasma for 5 min (PDC-001-HP–115 V from Harrick Plasma) to ensure that the substrates are thoroughly clean. The cleaned substrates were chemically treated with dopamine to enhance the contact line pinning of the jetted droplets by the following procedure: the cleaned glass slides were vertically immersed in a freshly prepared dopamine aqueous solution (5 mg/mL) with pH buffer of 8.5 (1.2 mg/mL tris) to initiate the oxidative self-polymerization reaction; after 24 h reaction, the substrates were rinsed with ethanol and DI water successively to remove the physically unattached dopamine particles and dried at 40 °C for 10 min using a vacuum oven (89508–426, 600W from VWR).

2.3. Ink preparation

The as-received suspensions of polystyrene particles were ultra-sonicated for 5 min to ensure a homogeneous suspension of the nanoparticles. Then, the suspensions were diluted by ethanol to obtain the inks for wetting droplets with a particle concentration of 10 mg/mL. The suspension was ultra-sonicated for another 5 min before printing. The ink for supporting droplets is DI water, the pH value of which is adjusted either by adding HCL or NaOH with known concentrations.

2.4. Dual-droplet inkjet printing process

The inkjet printing platform (Jetlab 4, MicroFab) consists of four printing stations, two of which were used in this study. Supporting droplets and wetting droplets were jetted from two piezoelectric nozzles with different orifice sizes of 30 μm (MJ-ATP-01-80-8MX, MicroFab) and 80 μm (MJ-ATP-01-30-8MX, MicroFab) driven by a waveform generator (Jetdriver III, MicroFab). In brief, a supporting droplet was generated by jetting multiple bursts of DI water with a total volume of ~110 nL on the substrate at a frequency of 500 Hz. Then, wetting droplets containing PS nanoparticles were jetted to the center of the supporting droplet using the 80 μm nozzle at a frequency of 1 Hz. This ensures a complete impact and spreading of the wetting droplet before subsequent droplets. In this work, we have used a jetting speed of ~1.3 m/s and a droplet volume of ~550 pL (diameter ~100 μm) for the wetting droplets.

2.5. Morphology characterization

An ultra-high-resolution scanning electron microscope (HITACHI SU-70 FE-SEM) with 5 kV and 15 mm scanning distance was used for morphology characterization of the printed patterns. To minimize charging effect of the PS nanoparticles, the samples were coated with platinum using a platinum sputter (Denton Vacuum Desk V) for 60 s.

2.6. Surface profilometry

Height profiles of the nanoparticle deposits were characterized using a stylus profilometer (Dektak 150, Veeco) with a stylus diameter of 12.5 μm. The measurements were recorded using a stylus force of 2 mg, scanning resolution of 0.1 μm, and scanning length of 2 mm.

2.7. Zeta potential characterization of colloidal nanoparticles and dopamine-coated substrates

The PS particles were dispersed in water with different pH values, which were adjusted either by adding HCL or NaOH with known concentrations. Zeta potential measurements were conducted using Malvern zetasizer (ZS). The pH value of the suspensions was measured by a benchtop pH meter (sensION + MM374, HACH, USA) with accuracy of ±0.1 pH. The zeta potential of the dopamine-coated glass slide was determined by an electrokinetic analyzer (SurPASS 3, Anton Paar, USA). Streaming current measurements were performed in asymmetric mode using a clamping cell. 1 mM KCL solution was used as the measuring electrolyte where 0.05 M of HCL and 0.05 M of NaOH were utilized to adjust the pH range accordingly. Three repetitions of zeta potential measurements were performed at each pH value for each tested sample.

3. Results and discussion

3.1. Self-assembly of nanoparticles at different pH values

Very recently, we have successfully demonstrated a nearly monolayer, closely-packed deposition of colloidal nanoparticles through a dual-droplet inkjet printing process. Nanoparticle-laden wetting droplets were jetted over a supporting droplet which was firstly deposited. Regulating surface tensions, droplet speeds, and droplet volumes resulted in effective particle spreading over the interface of the supporting droplet. The dynamics of wetting droplet impacting the supporting droplet, spreading of nanoparticles, and drying of solvents were discussed in detail in our earlier report [29]. In this study, we conducted a systematic investigation of particle-particle, particle-interface, and particle-substrate interactions initiated by the pH change of the supporting droplet in the dual-droplet inkjet printing. The supporting droplet was generated by multiple bursts of inkjet droplets that is equivalent to ~110 nL of water. One and three wetting droplets with a single droplet volume of ~550 pL were deposited onto the supporting droplet by a secondary printhead. In all the experiments, the modified Weber number (We') is controlled below 0.42 to ensure the spreading of the wetting droplet on the surface of the supporting droplet [29,30].

Fig. 1 illustrates the complex multibody interactions presented by the negatively charged PS particles accompanied with pH variation in the supporting droplet. Upon the wetting droplet impact on the supporting droplet, the PS particles spread on the interface of the supporting droplet. Consequently, the particles experience various types of interactions such as particle-interface and particle-particle interactions where the capillary forces compete with the particle electrostatic interactions and the particles' water affinity at the interface to facilitate the skin formation of PS particles. The self-assembly process is strongly influenced by the protonation and deprotonation of the supporting droplet, which in turn controls the surface charge magnitude of the particles at the interface. In this study, carboxyl- and sulfate-functionalized PS nanoparticles are selected because the former is sensitive to the pH change due to protonation and deprotonation of the carboxyl group while the latter is not. The protonation and deprotonation of the carboxyl group follows the reversible reaction equation, $R-\mathrm{COOH}_{aqueous} \leftrightarrow R-\mathrm{COO}^{-}_{aqueous} + \mathrm{H}^{+}_{aqueous}$. For pH = 7, the reaction to the right and the reverse reaction to the left reach an equilibrium with a certain concentration of $R-\mathrm{COO}^{-}$ in the system. When the solution is more acidic (pH < 7), more H^{+} protons present in the system, pushing the reverse reaction to the left and leading to a suppressed $R-\mathrm{COO}^{-}$ formation. Both the prominence of H^{+} protons and suppression of $R-\mathrm{COO}^{-}$ formation contribute to the significant decrease in the zeta potential (absolute value) in acidic environments. For pH > 7, the opposite trend, i.e., less protons and promotion of $R-\mathrm{COO}^{-}$ formation, is obtained leading to an increase in the zeta potentials (absolute value) of the carboxyl-PS particles. On the other hand, the sulfate group ($R-\mathrm{SO}_4^{-}$) is not affected by the concentration of the H^{+} in the system. At various pH conditions, zeta potential of the sulfate-PS particles changes as a result of the changing proton concentrations. Zeta potential measurements of suspensions with carboxyl- and sulfate-functionalized PS nanoparticles also support this analysis. As shown in Fig. 2, the zeta potential of carboxyl- and sulfate-PS nanoparticles show similar trends where the net negative charges of the particles decrease with the decrease in pH value, and vice versa. However, carboxyl-PS nanoparticles experience more drastic changes compared to the sulfate-PS particles, due to the above-mentioned protonation and deprotonation process. None of the colloidal suspensions reaches the isoelectric point (IEP) even when the pH value is dropped to 1.5. This observation is consistent with the results reported elsewhere [31].

In this study, the printing conditions are tuned so that the wetting droplets would not impinge into and mix with the supporting droplets. The wetting droplets carrying the colloidal nanoparticles successfully spread over the interface of supporting droplets, as a result of an instantaneous Marangoni flow due to the surface tension gradient emanated from the initial mixing of solvents upon the impact. Both carboxyl and sulfate functional groups have strong affinity to water, and the functionalized PS nanoparticles would diffuse and mix into the supporting droplet if no other forces prevent them from this process. Upon the wetting droplet spreading, capillary forces arise to compete against the interparticle electrostatic repulsion forces at the interface to push these nanoparticles to bridge and eventually agglomerate together forming various sizes of monolayer networks. Compared to individual spherical nanoparticles, these monolayer "islands" are trapped at the interface in an energetically favorable state due to the interfacial deformation caused by the fractal shape of the agglomerates [32]. Therefore, the nanoparticles at the interface may experience two different and competing movements: (i) particle diffusion and mixing into the supporting droplet, and (ii) particle assembling into "islands" of monolayer networks at the interface, which are determined by the capillary interactions of particle-particle and particle-interface, particle-particle electrostatic interactions, and particles' affinity to water [33]. When pH value of the supporting droplet changes, the particle-particle electrostatic force varies (Fig. 2) which correspondingly affects the assembly process at the interface and final deposition on the substrate.

Depending on the type of PS particles and the pH value utilized, various assembly structures of nanoparticle deposits are obtained from a nearly monolayer with well-ordered structures to relatively uniform but less-ordered deposits, and to depositions with ring-like morphologies. More details are presented in the following sections.

It is worth pointing out that for sulfate-PS nanoparticles at pH 7, besides the monolayer deposition in most of the deposits, a ring of nanoparticles was observed at the edge of the deposits, which is attributed to the nanoparticles at the interface interacting with the dopamine-coated substrate. When the pH changes from an acidic to a basic environment, as shown in Fig. 2, the zeta potential of the dopamine-coated substrate also varies from positive to negative, with an isoelectric point at pH 6.2. As a result of the particle-substrate interaction, the pH value of the supporting droplet strongly affects the morphology of the final deposits.

3.2. Effect of pH on deposit morphology of carboxyl-PS nanoparticles

To elucidate the mutual effect of the multibody interactions experienced by carboxyl-PS particles during the assembly, pH

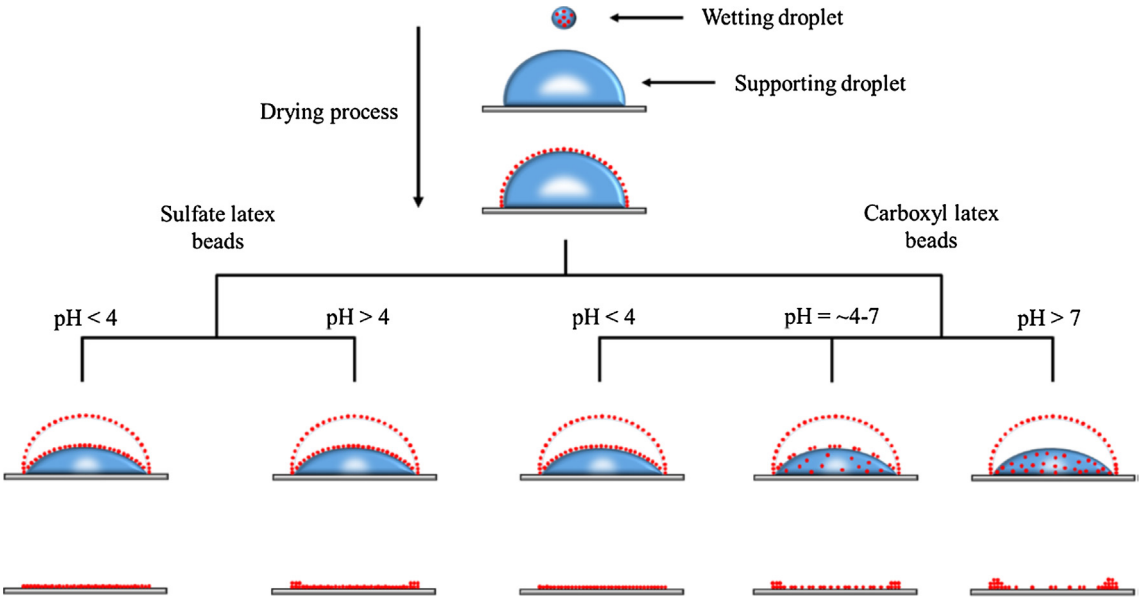

Fig. 1. Schematic of the dual-droplet inkjet printing where different interparticle and particle-substrate interactions are initiated at the interface and in the bulk of the supporting droplet. As the solvent evaporates, different deposition patterns are obtained depending on the type of the nanoparticles utilized and the pH value of the supporting droplet.

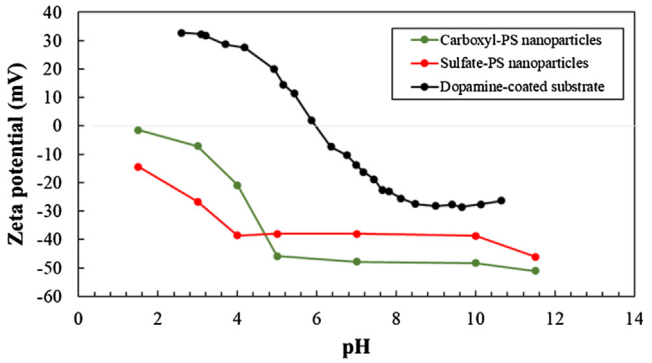

Fig. 2. The measured zeta potentials of carboxyl- and sulfate-PS particles in water and surface zeta potential of the dopamine-coated glass slide with respect to different pH values. The standard deviations for the colloidal particles and the dopamine-coated substrates are ~1 mV and ~3 mV, respectively.

values of the supporting droplets were systematically controlled. As illustrated in Fig. 1, the carboxyl-PS particles assemble differently according to the pH value utilized. For pH conditions of <4, ~4–7, and >7, nearly monolayer depositions without ring formation, non-uniform deposition with ring formation, and exclusive ring formation are obtained, respectively. The morphologies of the deposits composed of carboxyl-PS particles at various pH values are presented in Fig. 3 for one wetting droplet. The self-assembly mechanism and multibody interactions are illustrated in Fig. 4a and elaborated in detail as follows.

The assembly of the carboxyl-PS particles was first examined with a supporting droplet of pH 7. It is worth noting that when the self-assembled "islands" at the interface deposit onto the substrate, structural colors are generated due to the well-ordered periodic structures among the nearly monolayer nanoparticle assembly. On the other hand, lack of the structural colors indicates no ordered assembly present in the deposits. As shown in Fig. 3, no structural color exhibits in the nanoparticle deposition at pH 7. We deduce that most of the spreading nanoparticles diffuse into the bulk of the supporting droplet due to their strong hydrophilicity and strong particle-particle electrostatic repulsion forces (with a zeta potential of −47.8 mV), which inhibits the network formation at the interface. Some of the particles inside the supporting droplet are carried by the evaporation-induced flow to the edge of the sessile droplet while the rest are deposited inside the footprint due to particle-substrate interactions. Even though the dopamine-coated substrate shows the isoelectric point near pH of 6–7, it is hypothesized that the adsorbed zwitterionic dopamine has the ability to catch nanoparticles in the bulk of the supporting droplet by DLVO interactions [34]. The final deposition (Figs. 3 and S1) exhibits a non-uniform irregular morphology contributed mostly by the particles diffusing into the bulk of the supporting droplet.

When the supporting droplet gets more acidic (e.g. pH 5), the surface charge on the carboxyl-PS slightly decreases with a zeta potential of −45.9 mV. Upon the wetting droplet spreading on the supporting droplet, a small fraction of the nanoparticles survive and stay at the interface during the evaporation due to the slightly decreased interparticle electrostatic repulsion force. As shown in Fig. 3, agglomerate islands (bluish color[1]) are observed on top of the final deposits, which are attributed to the self-assembled floating "islands" of nanoparticles at the interface. A darker brown color of the deposition indicates that the nanoparticles inside the supporting droplet are captured by the dopamine-coated substrate, due to the particle–substrate attractive force, noticing that the dopamine-coated substrate has a positive zeta potential at pH 5 (14.4 mV).

When the pH value of the supporting droplets further decreases, e.g. pH 4, the protonation reaction of the carboxyl group is further suppressed, resulting in a large decrease in zeta potential (−20.9 mV). Such a condition facilitates more nanoparticles to be self-assembled and trapped at the interface while still a large number of nanoparticles diffuse and mix into the bulk of the supporting droplet. As shown in Fig. 4a, these nanoparticles experience strong particle-substrate electrostatic interactions (attractive force) that assists in trapping some of the particles in the middle of the deposit while the rest of the particles are carried to the three-phase contact line by the evaporation-induced capillary flow. As

[1] For interpretation of color in Figs. 3 and 5, the reader is referred to the web version of this article.

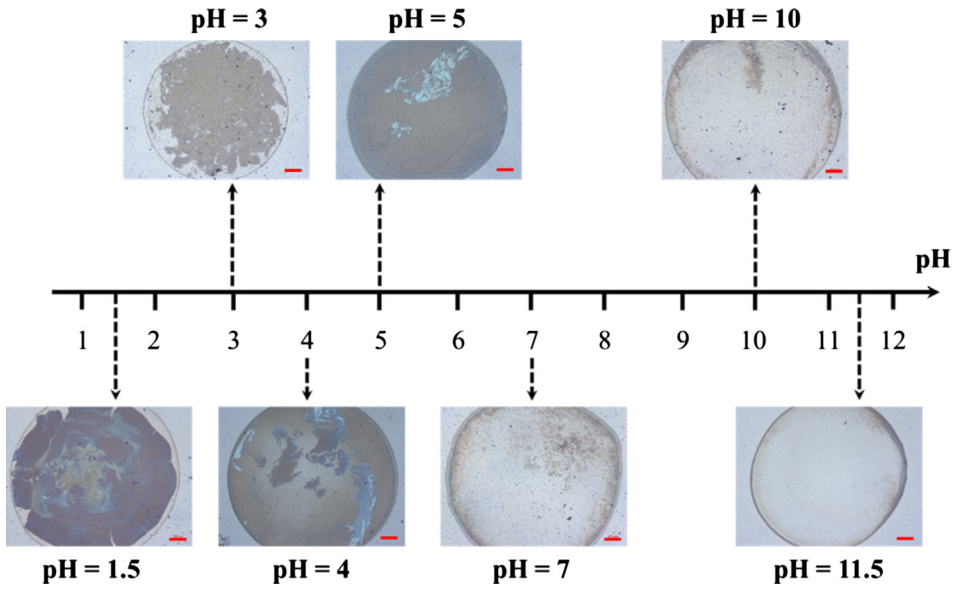

Fig. 3. Deposit patterns obtained from jetting one wetting droplet with carboxyl-PS particles on supporting droplets with different pH values. The scale bar is 100 μm.

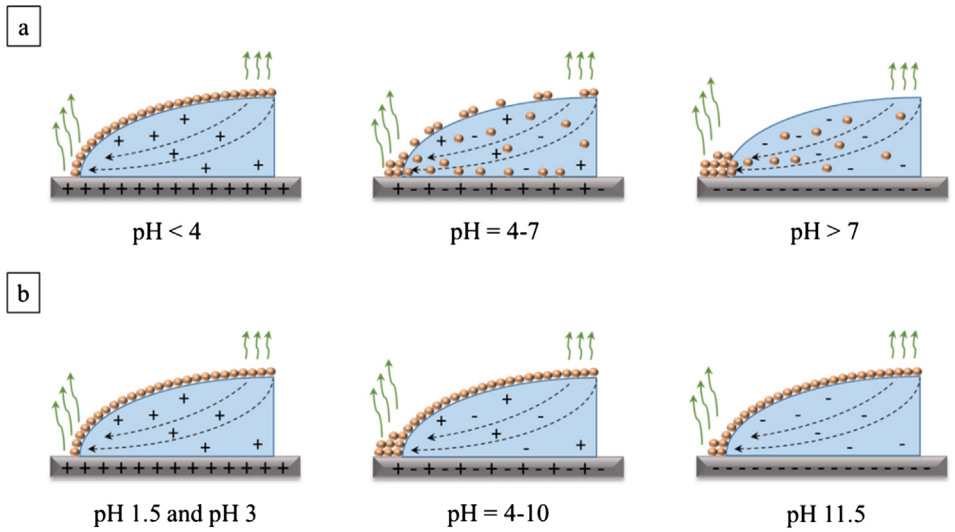

Fig. 4. Illustration of the multibody interactions at different pH values for (a) carboxyl-PS particles, and (b) sulfate-PS particles. The positive and negative signs represent ions available in the supporting droplet at various pH values.

a result, the final deposition obtained at pH 4 is composed of self-assembled particles at the interface of the supporting droplet, which is indicated by the bluish color, and the particles diffusing into the bulk during solvent evaporation that presents the brown color as shown in Fig. 3. This behavior is more pronounced at a higher particle loading such as jetting three wetting droplets (Fig. S1 in the Supporting Information).

A drastic change in the nanoparticle assembly is observed when the pH value decreases to 3 with a zeta potential of −7.2 mV. Due to the significantly decreased electrostatic repulsion between the nanoparticles, they tend to form agglomerates at the interface. On one hand, the agglomerates prevent the nanoparticles from diffusing and mixing into the supporting droplet as described earlier, and majority of the particles are trapped at the interface during the evaporation; on the other hand, the agglomerates are formed in a 3D configuration instead of a monolayer network. No structural colors are exhibited in the deposition due to lack of regular and periodic arrangement among the nanoparticle assembly.

When the pH of the supporting droplet is further reduced to 1.5, the carboxyl-PS particles exhibit the lowest surface charge (−1.43 mV) that results in minimal particle-particle electrostatic repulsions. In this case, the interparticle capillary forces (and possibly van der Waals forces) are strong enough to dominate the self-assembly process of nanoparticles at the interface. Interestingly, in this strong acidic environment, the nanoparticles may experience "melting and bridging" to form a nearly monolayer film of joined nanoparticle branches, as shown in Fig. S3 in the Supporting Information. No such melting behavior is perceived at pH values equal to or higher than 3. Although the supporting droplets and the substrate are strongly positively charged at this low pH value, their influences are not significant since all the particles prefer to stay at the interface (Fig. 4a) because of the weak interparticle repulsion interactions.

Compared to the condition of pH 7, zeta potential of the carboxyl-PS particles slightly increases when the supporting droplet becomes basic with pH values higher than 7. Interactions

among the charged particles at the interface, both negatively charged particles and dopamine-coated substrate result in similar yet still distinct deposit morphologies as shown in Fig. 3. For conditions of pH 7 and pH 10, due to the minimal difference in zeta potentials of the nanoparticles (~0.5 mV), we hypothesize that the particles behave in a similar fashion at the interface, i.e., most of the particles diffusing and mixing into the supporting droplet and only a very small population of particles floating at the interface. Nonetheless, the particles diffusing into the bulk of the supporting droplet exhibit a different behavior. Notice the zeta potential of the substrate increases to (−27.5 mV) in the basic environment. In this case, in addition to the evaporation-induced flow, which carries those particles to the contact line of the supporting droplet, they also experience stronger particle-substrate repulsion forces that ease the particle migration to the contact line. Fig. 4a illustrates the multibody electrostatic interactions at pH > 7. Although all the mechanisms push the particles to migrate to the edge of the supporting droplet, some of them could be observed in the middle of the deposits after the drying process. This could be attributed to: (i) zwitterionic polymer (dopamine) adsorbed on the substrate surface attracts some negatively charged PS particles, and (ii) we hypothesize that some PS particle might be trapped by the substrate surface roughness during their migration path to the edge of the supporting droplet. Surprisingly, no particles are deposited in the middle of the footprint when pH 11.5 is utilized (Fig. S3 in the Supporting Information). In this case, the substrate, the supporting droplet, and the PS particles are all highly negatively-charged. This exemplifies a scenario that upon the particles spreading on the interface, they fail to assemble into agglomerates or networks at the interface due to strong interparticle repulsion interactions; instead, they diffuse and mix into the supporting droplets due to their strong hydrophilicity. Furthermore, all these particles transport to the edge of the supporting droplet by the action of the evaporative-induced capillary flow. Due to the strong particle-substrate repulsion interactions, all these particles could not deposit onto the substrate until they reach the contact line of the supporting droplet, producing the conventional "coffee-ring" effect.

3.3. Effect of pH on deposit morphology of sulfate-PS nanoparticles

To assess the effect of pH on the sulfate-PS particle assembly, the pH of the supporting droplet was systematically adjusted from 1.5 to 11.5. Figs. 1 and 4b illustrate the effect of pH on the deposits produced by sulfate-PS particles and multibody interactions involved in this assembly process. Sulfate functional groups are the most hydrophilic in nature due to their acidity. However, the sulfate-PS particles in this study have only about ~1/12th functional groups per particle of those on the carboxyl-PS particles (Table S1). Fewer functional groups and lower zeta potentials lead to weaker interparticle repulsion interactions and less affinity to water, which facilitates the skin formation at the interface and correspondingly reduces the number of nanoparticles diffusing into the supporting droplet. Yet, fewer functional groups on the particle and less surface charge density are also responsible for more particle agglomerations as compared to the carboxyl-PS particles (Fig. S4 in the Supporting Information). The sulfate-PS particles gave strikingly different outcomes from the carboxyl counterparts when utilizing various pH values in the supporting droplet. Such nanoparticles are less prone to the pH change where the fully covered, nearly monolayer deposition is always the case (Fig. 5). At pH 11.5, the sulfate-PS particles have a zeta potential of −46.1 mV which is comparable to that of carboxyl-PS particles at the pH 4. However, the sulfate-PS particle's affinity to water is much weaker than its counterpart due to the fewer sulfate functional groups on the PS particles. As a result, even at this most basic condition and with the strongest interparticle repulsive interactions, the sulfate-PS particles successfully self-assemble into nearly monolayer networks at the interface and deposit the well-ordered assembly onto the substrate upon solvent evaporation. The bluish structural color exhibited in Fig. 5 indicates the high quality and orderliness of the particle assembly, which stems from the periodic optical cavities in the depositions produced at different acidic and basic environments. The optical images in Fig. 5 and the SEM images in Fig. S4 support the hypothesis that in all the pH conditions, the sulfate-PS particles self-assemble into monolayer networks at the interface, maintaining the well-ordered assembly structure until final deposition, despite the change in zeta potentials.

Differences, however, do exist in the deposition morphology of the sulfate-PS particles at various pH conditions. At pH 1.5, akin to the carboxyl-PS particles, the sulfate-PS particles "melt" and join each other at the interface, forming a solid skin of nanoparticles, during the drying process. This behavior is observed at pH 1.5 even though the sulfate functional groups are not pH sensitive. Further increase in pH value (e.g., pH 4 and 5 with zeta potentials ~−38 mV) has led to higher interparticle repulsion interactions by which

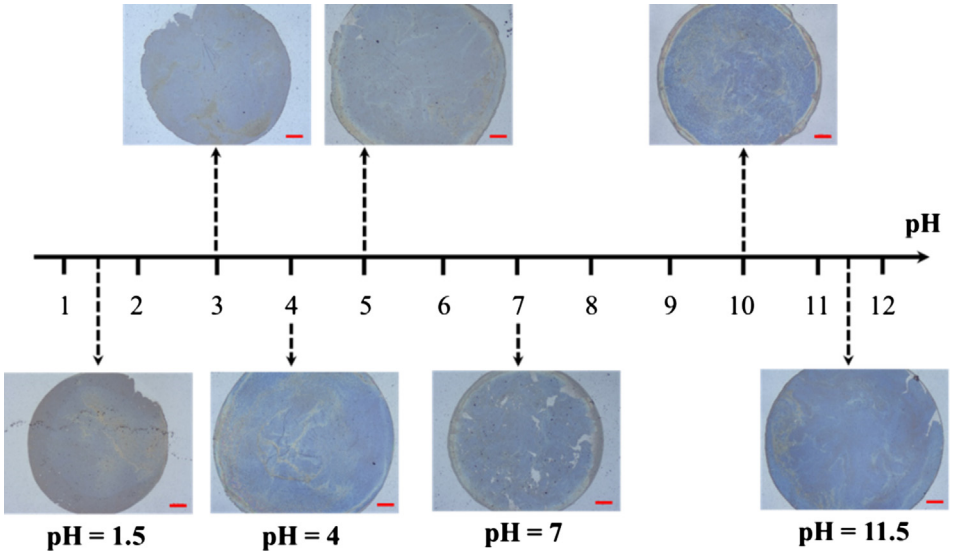

Fig. 5. Deposit patterns obtained from jetting one wetting droplet with sulfate-PS particles on the supporting droplets with different pH values. The scale bar is 100 μm.

the close-packing of the nanoparticles is slightly affected as shown in the Supporting Information (Fig. S4). However, the capillary force present at the interface of the supporting droplet still prevails the other forces. The dopamine-coated substrate at such pH levels is highly, positively charged that attracts the excess amount of the floating particles at the interface contributing to the ring formation (Fig. 4b). The ring-like pattern can be clearly seen at a larger particle loading, e.g. three wetting droplets, as shown in Fig. S2. It should be noted that the ring formed of sulfate-PS particles originates from particles trapped at the interface of the supporting droplet. While the ring composed of carboxyl-PS particles, especially at pH > 3, is a combination of the particles diffusing into the bulk and the particles at the interface of the supporting droplet.

When the pH of the supporting droplet increases to 6 or 7, the zeta potential of the nanoparticles does not change much (∼−38 mV), while the dopamine-coated substrate exhibits an isoelectric point at pH 6.2. As described in the previous section, the positively charge amine groups could capture the negatively charged PS particles even though the overall charge on the dopamine-coated substrate is neutral. This provides an explanation to the ring formed at this particular pH value.

A repulsion force arises between the particles and the substrate at pH > 7, where the substrate, the supporting droplet, and the nanoparticles are all negatively charged. This repulsion force reduces the amount of the nanoparticles deposited at the ring by forcing them back to the surface of the supporting droplet (more details are provided in Section 3.4). Further increasing the pH to 11.5 has boosted the particle-substrate repulsive interactions (Fig. 4b) where the surface charges become highly negative. The basic solution not only significantly reduces the amount of the particles deposited at the ring, but also enhances the formation of highly-ordered, closely-packed monolayers of nanoparticle assembly by squeezing the nanoparticles back to the interface. Consequently, the blue color contrast is the brightest at pH 11.5. The SEM images of the deposits are presented in Fig. S4 in the Supporting Information.

Finally, because the sulfate-PS particles are more robust against the pH change where most of the particles remain trapped at the interface of the supporting droplet, buckling and folding of formed skins have been observed at higher particle loadings (e.g. three wetting droplets). A similar observation of the film buckling phenomenon at high particle loadings have been reported by Boley et al. [35]

3.4. Discussion

In this dual-droplet printing process, the final structure of the particle assembly depends on the particle affinity to water (type of functional groups and density), the charge level of the PS particles (zeta potential), and the pH of the supporting droplet. For sulfate-PS particles, much fewer functional groups per particle make the particles less hydrophilic. Even when the zeta potential increases to −46.1 mV and the sulfate-PS particles experience strong electrostatic repulsion, they still self-assemble into monolayer networks at the interface. On the other hand, carboxyl-PS particles are much more hydrophilic due to the large number of functional groups on the particle surface. Self-assembly of carboxyl-PS particles is only obtained for zeta potential of −7.2 mV or lower, corresponding to pH of 3 or less. As the zeta potential increases (along with the increase in pH), less carboxyl-PS particles can self-assemble and maintain at the interface. When the zeta potential increases to −51.1 mV (at pH 11.5), no particles survive at the interface during the evaporation; and instead, all the particles diffuse and mix into the supporting droplet.

When the sulfate-PS particles are trapped at the interface during the evaporation, they maintain the well-ordered assembly structure and deposit onto the substrate upon drying. However, very small amount of particles still get captured by the dopamine surface at the contact lines of the supporting droplet, especially for conditions of pH 4–10. Dopamine surface has a positive zeta potential for pH < 6. This means that the negatively charged PS particles at the interface can be attracted to the contact line and deposited at the edge due to electrostatic interactions. Furthermore, dopamine is a zwitterionic polymer which is capable of attracting some negatively charged PS particles at the interface, even when its zeta potential is negative (for pH of 7–10). As a result of this deposition, a ring forms at the edges of the supporting droplet (Figs. S2 and S5). In addition, the particles diffusing and mixing into the supporting droplet also contribute to the ring formation, particularly for carboxyl-PS particles (Figs. S1 and S5). Those particles follow the evaporation-induced capillary flow inside the supporting droplet and move towards the contact line. During their journey, some particles may get captured and randomly deposit on the dopamine-coated substrate due to the aforementioned electrostatic interactions, zwitterionic nature of the dopamine surface, and/or roughness of the dopamine surface. The rest of the particles deposit near the edges of the supporting droplet. When the zeta potential of the dopamine surface increases to −28.5 mV for pH > 10, the negatively charged particles could not deposit onto the dopamine surface due to strong electrostatic repulsion. Therefore, for the extreme case of carboxyl-PS particles at pH 11.5, all the particles diffusing into the supporting droplet are repelled by the substrate and accumulated near the edges of the supporting droplet, producing the conventional coffee ring.

Fig. 6a illustrates the height profile of the carboxyl-PS particle deposits measured by the profilometer. At low pH values (e.g. pH 1.5 and pH 3), the floating particles at the interface of the supporting droplet have low charges that eases the network formation by the action of capillary forces. The particles are held firmly in their network where a negligible amount of particles deposit onto the dopamine surface at the contact line regardless the favorable attractive electrostatic force between the particles and the dopamine-coated substrate. Therefore, the rings at the low pH values have negligible thicknesses. The ring is measured to be ∼1 μm in height at pH 4. When the pH further increases, the rings become thicker and wider, reaching ∼2 μm in height for pH 10. This growth is contributed by the particles from both the interface and the bulk of the supporting droplet. While for pH 11.5, the ring turns into a narrow and tall peak (3.3 μm in height) since all the particles exclusively deposit near the edges and no particles in the middle of the deposit due to the strong repulsion from the dopamine-coated substrate.

On the other hand, the sulfate-PS particles are less susceptible to pH change where the interface of the supporting droplet is always covered with the self-assembled nanoparticles. Fig. 6b presents the height profile of deposits with sulfate-PS nanoparticles. Since the sulfate-PS particles successfully self-assemble at the interface with negligible particles mixing into the supporting droplet, the ring formed with the sulfate-PS particles is dominantly from the particles at the interface. Similar to the carboxyl nanoparticles, low pH values (e.g. pH 1.5 and pH 3) give monolayers of sulfate-PS particles and no accumulation of particles at the contact lines. An increase in particle loading (i.e. three wetting droplets) did not produce a ring (Fig. S2 in the Supporting Information). Instead, we have observed that jetting more wetting droplets creates a hole in the self-assembled film and induces vortices close to the interface of the supporting droplet. Analogous observation of such eddies has been reported by Parsa et al. in an effort to study the effect of substrate temperature on pattern formation [11]. However, the ring starts to develop at pH 4 due to the increase in the attractive electrostatic interactions between the particles at the interface and the dopamine-coated substrate at the contact

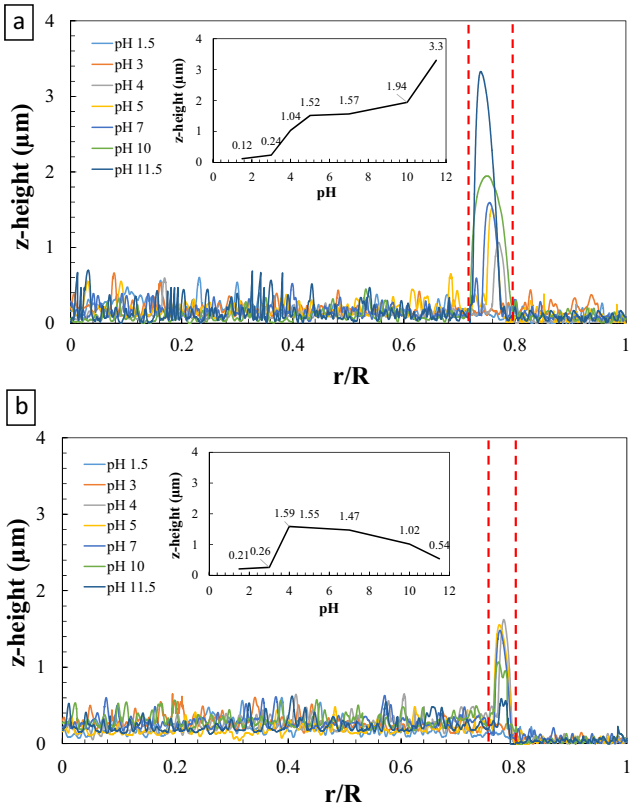

Fig. 6. Height profiles near the deposit edges obtained from dual-droplet printing of (a) carboxyl-PS particles, and (b) sulfate-PS particles at different pH values. The red dash lines represent the ring region while the inset shows the z-height of each individual peak with its corresponding pH value. (For interpretation of the references to color in this figure legend, the reader is referred to the web version of this article.)

line. The rings are very similar among the deposits in pH values between 4 and 7 with the highest peak of ~1.6 μm. The situation significantly changes at pH 11.5. The substrate becomes highly negatively charged that pushes the nanoparticles near the contact line back to the interface of the supporting droplet resulting in a monolayer assembly with a higher degree of closely-packed deposition. Consequently, the amount of nanoparticles present in the ring of the deposit significantly reduces, which is contrary to the rings obtained at the same pH level with carboxyl-PS particles. Both Fig. 6a and b show some peaks (~0.5 μm) in the middle of the deposits that correspond to PS particles (particularly the sulfate-PS particles) and dopamine agglomerates.

4. Conclusion

In this work, we have demonstrated controlling deposition morphology in the dual-droplet inkjet printing by pH-modulation along with the associated electrostatic interactions of nanoparticles. It is worth emphasizing that majority of the prior research efforts on colloidal particle deposition from a droplet are based on a homogeneous particle-laden sessile droplet ranging from tens of microns to millimeter size in diameter. Various approaches have been employed to alter the evaporation-induced flow field, particle-particle, and particle-substrate interactions resulting in different deposition morphology of the colloidal particles, e.g. dome-shape depositions [36], line patterns [37], spider web and radial spoke structures [38], relatively uniform depositions with suppressed coffee-ring formation [11–17] etc. However, depositions with nearly a monolayer of self-assembled colloidal particles have rarely been obtained. Recent efforts have been made to push the colloidal particles to the droplet interface during the solvent evaporation, leading to some well-ordered depositions [39–41]. Different from these depositions from particle-laden sessile droplets, interfacial self-assembly is the driving mechanism in the deposition formation during the dual-droplet printing. The colloidal particles are spread on the air-water interface of the supporting droplet when the wetting droplet impacts onto the supporting droplet. The self-assembly of the particles occurs at the interface, and in favorable conditions maintains at the interface during the solvent evaporation, till finally deposits onto the substrate. pH modulation of the supporting droplet affects the interfacial self-assembly through multibody interactions among the nanoparticles, and the particle-interface and particle-substrate interactions. The final structure of the particle assembly is determined by the particle affinity to water (type of functional groups and density), charge level of the PS particles (zeta potential), and the pH of the supporting droplet.

The carboxyl-PS particles have higher affinity to water and is more prone to pH change. At pH values as low as 3, the particles tend to self-assemble at the interface of the supporting droplet, where the interparticle interactions are minimal due to the low surface charge. However, they diffuse and mix into the supporting droplet as the pH increases. For extreme pH values (i.e. pH 10 and pH 11.5), most of the particles at the interface diffuse into the supporting droplet where they are carried by the evaporation-induced capillary flow to the contact line producing the conventional coffee-ring. The sulfate-PS particles, on the other hand, is marginally affected by the pH change. Its low surface charge density facilitates the self-assembly of the nanoparticles at the interface of the supporting droplet regardless of the pH value utilized. Contrary to the carboxyl-PS particles, the sulfate-PS particles, even at extreme basic and acidic environments, successfully self-assemble into nearly monolayer networks at the interface and deposit the well-ordered assembly onto the substrate upon solvent evaporation. Finally, reducing the pH value of the supporting droplet to 3 or less produces self-assembled networks regardless the type of nanoparticles employed where no ring formation is observed.

Future works include investigating the interfacial self-assembly of anisotropic colloidal nanoparticles in the dual-droplet inkjet printing process; and employing functional materials (e.g. noble metals) to fabricate low-cost, high-performance functional devices, e.g. surface enhanced Raman scattering (SERS) substrates. Incorporating the scalable dual-droplet inkjet printing technique with the ability to control the assembly structures of the deposits can become a promising approach to printing functional optical and electronic devices.

Acknowledgments

The authors are grateful for the support of the National Science Foundation (CMMI-1634938). We also would like to thank Dr. Christina Tang for the access of Malvern zetasizer and insightful discussions.

Appendix A. Supplementary material

Supplementary data associated with this article can be found, in the online version, at https://doi.org/10.1016/j.jcis.2018.06.008.

References

[1] T.A.H. Nguyen, M.A. Hampton, A.V. Nguyen, Evaporation of nanoparticle droplets on smooth hydrophobic surfaces: the inner coffee ring deposits, J. Phys. Chem. C 117 (2013) 4707–4716.

[2] Z.S. Davidson, Y. Huang, A. Gross, A. Martinez, T. Still, C. Zhou, P.J. Collings, R.D. Kamien, A.G. Yodh, Deposition and drying dynamics of liquid crystal droplets, Nat. Commun. 8 (2017) 15642.
[3] D. Liu, C. Li, F. Zhou, T. Zhang, G. Liu, W. Cai, Y. Li, Capillary gradient-induced self-assembly of periodic au spherical nanoparticle arrays on an ultralarge scale via a bisolvent system at air/water interface, Adv. Mater. Interfaces 4 (2017) 1600976.
[4] P. Jiang, J.F. Bertone, K.S. Hwang, V.L. Colvin, Single-crystal colloidal multilayers of controlled thickness, Chem. Mater. 11 (1999) 2132–2140.
[5] S. Wong, V. Kitaev, G.A. Ozin, Colloidal crystal films: advances in universality and perfection, J. Am. Chem. Soc. 125 (2003) 15589–15598.
[6] M. Anyfantakis, D. Baigl, Manipulating the coffee-ring effect: interactions at work, ChemPhysChem 16 (2015) 2726–2734.
[7] R.D. Deegan, Pattern formation in drying drops, Phys. Rev. E 61 (2000) 475–485.
[8] J. Sun, B. Bao, M. He, H. Zhou, Y. Song, Recent advances in controlling the depositing morphologies of inkjet droplets, ACS Appl. Mater. Interfaces 7 (2015) 28086–28099.
[9] R.D. Deegan, O. Bakajin, T.F. Dupont, G. Huber, S.R. Nagel, T.A. Witten, Capillary flow as the cause of ring stains from dried liquid drops, Nature 389 (1997) 827–829.
[10] W. Han, Z. Lin, Learning From "coffee Rings": ordered structures enabled by controlled evaporative self-assembly, Angew. Chem. Int. Ed. 51 (2012) 1534–1546.
[11] M. Parsa, S. Harmand, K. Sefiane, M. Bigerelle, R. Deltombe, Effect of substrate temperature on pattern formation of nanoparticles from volatile drops, Langmuir 31 (2015) 3354–3367.
[12] V.H. Chhasatia, A.S. Joshi, Y. Sun, Effect of relative humidity on contact angle and particle deposition morphology of an evaporating colloidal drop, Appl. Phys. Lett. 97 (2010) 231909.
[13] M. Majumder, C.S. Rendall, J.A. Eukel, J.Y.L. Wang, N. Behabtu, C.L. Pint, T.Y. Liu, A.W. Orbaek, F. Mirri, J. Nam, et al., Overcoming the "coffee-Stain" effect by compositional marangoni-flow-assisted drop-drying, J. Phys. Chem. B 116 (2012) 6536–6542.
[14] V.R. Dugyala, M.G. Basavaraj, Control over coffee-ring formation in evaporating liquid drops containing ellipsoids, Langmuir 30 (2014) 8680–8686.
[15] P.J. Yunker, T. Still, M.A. Lohr, A.G. Yodh, Suppression of the coffee-ring effect by shape-dependent capillary interactions, Nature 476 (2011) 308–311.
[16] Y.F. Li, Y.J. Sheng, H.K. Tsao, Evaporation stains: suppressing the coffee-ring effect by contact angle hysteresis, Langmuir 29 (2013) 7802–7811.
[17] S. Das, A. Dey, G. Reddy, D.D. Sarma, Suppression of coffee-ring effect: evaporation driven disorder to order transition in colloidal droplets, J. Phys. Chem. Lett. 8 (2017) 4704–4709.
[18] W. Sempels, R. De Dier, H. Mizuno, J. Hofkens, J. Vermant, Auto-production of biosurfactants reverses the coffee ring effect in a bacterial system, Nat. Commun. 4 (2013) 1757.
[19] C. Zhou, J. Han, R. Guo, A facile strategy to colloidal crystals by drying condensed suspension droplets, J. Colloid Interface Sci. 397 (2013) 80–87.
[20] E.L. Talbot, H.N. Yow, L. Yang, A. Berson, S.R. Biggs, C.D. Bain, Printing small dots from large drops, ACS Appl. Mater. Interfaces 7 (2015) 3782–3790.
[21] A. Marin, R. Liepelt, M. Rossi, C. Kaehler, Surfactant-driven flow transitions in evaporating droplets, Soft Matter 12 (2016) 1593–1600.
[22] H. Kim, F. Boulogne, E. Um, I. Jacobi, E. Button, H.A. Stone, Controlled uniform coating from the interplay of marangoni flows and surface-adsorbed macromolecules, Phys. Rev. Lett. 116 (2016) 124501.
[23] D.S. Eom, J. Chang, Y.W. Song, J.A. Lim, J.T. Han, H. Kim, K. Cho, Coffee-ring structure from dried graphene derivative solutions: a facile one-step fabrication route for all graphene-based transistors, J. Phys. Chem. C 118 (2014) 27081–27090.
[24] Y. Li, W. Zhang, J. Hu, Y. Wang, X. Feng, W. Du, M. Guo, B.F. Liu, Rapid assembly of large scale transparent circuit arrays using PDMS nanofilm shaped coffee ring, Adv. Funct. Mater. 27 (2017) 1606045.
[25] M. Layani, M. Gruchko, O. Milo, I. Balberg, D. Azulay, S. Magdassi, Transparent conductive coatings by printing coffee ring arrays obtained at room temperature, ACS Nano 3 (2009) 3537–3542.
[26] R. Bhardwaj, X. Fang, P. Somasundaran, D. Attinger, Self-assembly of colloidal particles from evaporating droplets: role of DLVO interactions and proposition of a phase diagram, Langmuir 26 (2010) 7833–7842.
[27] S. Devineau, M. Anyfantakis, L. Marichal, L. Kiger, M. Morel, S. Rudiuk, D. Baigl, Protein adsorption and reorganization on nanoparticles probed by the coffee-ring effect: application to single point mutation detection, J. Am. Chem. Soc. 138 (2016) 11623–11632.
[28] A. Zigelman, O. Manor, The deposition of colloidal particles from a sessile drop of a volatile suspension subject to particle adsorption and coagulation, J. Colloid and Interface Sci. 509 (2018) 195–208.
[29] K.N. Al-Milaji, R.R. Secondo, T.N. Ng, N. Kinsey, H. Zhao, Interfacial self-assembly of colloidal nanoparticles in dual-droplet inkjet printing, Adv. Mater. Interfaces 5 (2018) 1701561.
[30] Y. Noda, H. Minemawari, H. Matsui, T. Yamada, S. Arai, T. Kajiya, M. Doi, T. Hasegawa, Underlying mechanism of inkjet printing of uniform organic semiconductor films through antisolvent crystallization, Adv. Funct. Mater. 25 (2015) 4022–4031.
[31] H. Wang, V. Singh, S.H. Behrens, Image charge effects on the formation of pickering emulsions, J. Phys. Chem. Lett. 3 (2012) 2986–2990.
[32] J.C. Loudet, A.M. Alsayed, J. Zhang, A.G. Yodh, Capillary interactions between anisotropic colloidal particles, Phys. Rev. Lett. 94 (2005) 18301.
[33] T.P. Bigioni, X.-M. Lin, T.T. Nguyen, E.I. Corwin, T.A. Witten, H.M. Jaeger, Kinetically driven self assembly of highly ordered nanoparticle monolayers, Nat. Mater. 5 (2006) 265–270.
[34] L. Su, Y. Yu, Y. Zhao, F. Liang, X. Zhang, Strong antibacterial polydopamine coatings prepared by a shaking-assisted method, Sci. Rep. 6 (2016) 24420.
[35] J.W. Boley, S.H. Hyun, E.L. White, D.H. Thompson, R.K. Kramer, Hybrid self-assembly during evaporation enables drop-on-demand thin film devices, ACS Appl. Mater. Interfaces 8 (2016) 34171–34178.
[36] M. Kuang, J. Wang, B. Bao, F. Li, L. Wang, L. Jiang, Y. Song, Inkjet printing patterned photonic crystal domes for wide viewing-angle displays by controlling the sliding three phase contact line, Adv. Opt. Mater. 2 (2014) 34–48.
[37] M.A. Ray, H. Kim, L. Jia, Dynamic self-assembly of polymer colloids to form linear patterns, Langmuir 21 (2005) 4786–4789.
[38] X. Yang, C.Y. Li, Y. Sun, From multi-ring to spider web and radial spoke: competition between the receding contact line and particle deposition in a drying colloidal drop, Soft Matter 10 (2014) 4458–4463.
[39] J.W. Boley, S.H. Hyun, E.L. White, D.H. Thompson, R.K. Kramer, Hybrid self-assembly during evaporation enables drop-on-demand thin film devices, ACS Appl. Mater. Interfaces 8 (50) (2016) 34171–34178.
[40] Y. Li, Q. Yang, M. Li, Y. Song, Rate-dependent Interface Capture beyond the Coffee-ring Effect, Sci. Rep. 6 (2016) 24628.
[41] M. Anyfantakis, Z. Geng, M. Morel, S. Rudiuk, D. Baigl, Modulation of the coffee-ring effect in particle/surfactant mixtures: the importance of particle-interface interactions, Langmuir 31 (14) (2015) 4113–4120.